Dalton Transactions

ROYAL SOCIETY OF CHEMISTRY

PAPER

View Article Online
View Journal | View Issue

Cite this: *Dalton Trans.*, 2022, **51**, 18127

A *trans*-Pt(II) hedgehog pathway inhibitor complex with cytotoxicity towards breast cancer stem cells and triple negative breast cancer cells†

Aisling L. Ryan, [a,b] Joshua Northcote-Smith,[c] Aoife McKeon,[a] Andrew Roe,[d] Paul O'Dowd, [a,b] Brendan Twamley,[e] Triona Ní Chonghaile,[d] Kogularamanan Suntharalingam *[c] and Darren M. Griffith *[a,b]

The first example of a Pt complex of GANT61, a hedgehog (Hh) pathway inhibitor is reported. Reaction of *cis*-[Pt(II)Cl_2(dmso)$_2$] with one equivalent of 4-pyridine carboxaldehyde (4-PCA, control ligand) or one equivalent of GANT61 (Hh pathway inhibitor) in acetone at rt for 30 minutes afforded *trans*-[Pt(II)Cl_2(dmso)(4-PCA)] (**1**) and *trans*-[Pt(II)Cl_2(dmso)(GANT61)] (**2**) respectively, where 4-PCA and GANT61 are N-donor ligands. The structures of **1** and **2** were fully characterised by elemental analysis, ^{1}H NMR, ^{13}C NMR and IR spectroscopy and X-ray crystallography. **1** and **2** undergo isomerisation from *trans*- to *cis*-in solution and therefore the biological activity of **2** is also associated with the *cis*-configuration. The *in vitro* cytotoxicity data show that **2** is a potent inhibitor of the growth of breast CSC-depleted HMLER and breast CSC-enriched HMLER-shEcad cells. Furthermore **2** markedly reduced the size and viability and significantly reduced the number of CSC-enriched HMLER-shEcad mammospheres formed. **2** also induced apoptosis with low micromolar IC_{50} values against two triple negative breast cancer lines, MDA-MB-231 (MDA231) and BT549. **2**, which possesses the Hh pathway inhibitor GANT61 as an N donor ligand exhibits far superior anti-CSC activity including in the CSC-enriched mammosphere model and activity against TNBC cells as compared to its control analogue, the *trans*-Pt(II) 4-PCA complex **1**. The *trans*-Pt GANT61 complex **2** has also been shown to cause DNA damage and inhibit the Hh pathway at the level of GLI.

Received 1st September 2022,
Accepted 31st October 2022

DOI: 10.1039/d2dt02865d

rsc.li/dalton

Introduction

Platinum (Pt)-based compounds exhibit efficacy against many solid tumours and are in turn an important and established class of anticancer chemotherapeutics.[1]

The three Pt(II) anticancer drugs with worldwide approval, cisplatin, carboplatin and oxaliplatin, Fig. 1, are administered singularly or in anticancer regimens together with other anticancer agents such as doxorubicin, etoposide, gemcitabine, paclitaxel and 5-fluorouracil.[2]

The cytotoxicity of Pt anticancer drugs is primarily attributed to electrophilic Pt(II) centres covalently binding nuclear DNA, which induces DNA perturbation damage responses and ultimately programmed cell death, apoptosis. Pt(II) centres are also increasingly accepted to react with many cytoplasmic nucleophiles, including mitochondrial DNA, RNA as well as multiple mitochondrial and extramitochondrial proteins.[1]

Despite the unquestionable success of Pt(II) anticancer drugs, their clinical efficacy is limited by toxic side effects[3] and resistance (intrinsic or acquired).[4] The underlying resistance mechanisms are complex and include decreased accumulation, detoxification, increased DNA damage repair, and abnormal signaling pathways.[4,5]

Drug treatment failure and cancer relapse are also associated with the self-renewal properties associated with a small

[a]*Department of Chemistry, RCSI, 123 St. Stephens Green, Dublin 2, Ireland. E-mail: dgriffith@rcsi.com*
[b]*SSPC, Synthesis and Solid State Pharmaceutical Centre, Ireland*
[c]*School of Chemistry, University of Leicester, Leicester LE1 7RH, UK*
[d]*Department of Physiology and Medical Physics, Royal College of Surgeons in Ireland, Dublin, Ireland*
[e]*School of Chemistry, Trinity College Dublin, University of Dublin, Dublin 2, Ireland*

†Electronic supplementary information (ESI) available. CCDC 2196198 and 2196199. For ESI and crystallographic data in CIF or other electronic format see DOI: https://doi.org/10.1039/d2dt02865d

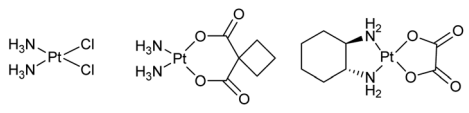

Fig. 1 Structures of cisplatin (*cis*-[Pt(II)$Cl_2(NH_3)_2$]), carboplatin ([Pt(II)(CBDCA$_{2H}$)$(NH_3)_2$], CBDCA = cyclobutane-1,1-dicarboxylic acid) and oxaliplatin ([Pt(II)(DACH)(Ox)] (DACH = 1*R*,2*R*-diaminocyclohexane, Ox = oxalato)).

population of tumour cells called cancer stem cells (CSCs). CSCs have the ability to differentiate, self-renew and seed the formation of new metastatic tumors at secondary sites.[5,6] Significantly CSCs are typically more resistant to chemotherapeutic agents, including Pt-based anticancer drugs, as compared to more differentiated cellular subtypes from the same tissue.[7,8] Therefore clinical Pt(II) anticancer drugs cannot effectively eradicate CSCs.

The Hedgehog (Hh) signalling pathway regulates cell differentiation, cell proliferation and stem cell maintenance during embryonic development. Signaling in the Hh pathway ultimately results in downstream transcription of three glioma-associated oncogene homologue (GLI) transcription factor proteins, GLI1, GLI2 and GLI3. GLI1 and GLI2 behave as activating proteins.[9] The Hh pathway is usually silent in adult tissues but abnormal Hh signalling does occur and is strongly associated with tumour growth, tumour resistance to drug treatment, and metastasis.[9,10] In addition, the Hh pathway plays a role in the maintenance and differentiation of CSCs including breast cancer stem cells (BCSCs).[11,12] Inhibition of the hedgehog pathway therefore represents an important therapeutic strategy to tackle resistance and target CSCs.

GANT61 is a small molecule inhibitor of the Hh pathway that acts downstream at the level of GLI. It has been shown to block GLI function in the nucleus, suppress both GLI1- and GLI2-mediated transcription, and inhibit the binding of GLI1 with DNA.[13,14] GANT61 exhibits antiproliferative/antitumour activity *in vitro* and *in vivo*[15,16] and was also demonstrated to attenuate stem cell phenotypes such as CD44+/CD24−ve cells and sphere forming capacity in triple negative breast cancer (TNBC) cell lines.[17] Significantly GANT61 hydrolyses *in vivo* to give 4-pyridine carboxaldehyde (4-PCA), GANT61-A, and the bioactive diamine derivative, GANT61-D (Scheme 1). GANT61-D is responsible for the inhibition of GLI-mediated transcription and is reported to bind to an active zinc finger site in GLI1.[18,19]

Previously we developed Ni(II), Pd(II), and Pt(II) complexes of the Hh pathway inhibitor GANT61-D, where the Ni(II) and Pd(II) complexes exhibited noteworthy *in vitro* cytotoxicity against medulloblastoma cancer cells.[20]

In this study we hypothesised that a Pt(II) Hh pathway inhibitor complex may target bulk tumour cells *via* Pt(II) DNA binding and subpopulations of cancer stem cells *via* Hh inhibition and in turn combat resistance in breast cancer.

Numerous preclinical and non-traditional classes of Pt anticancer drug candidates have been developed to date.[21] *trans*-[Pt(II)Cl_2(dmso)L] type complexes, where L is a planar N-donor aromatic ligand or heterocyclic ligand, exhibit appreciable anticancer activity though in most cases inferior activity as compared to cisplatin.[22–24]

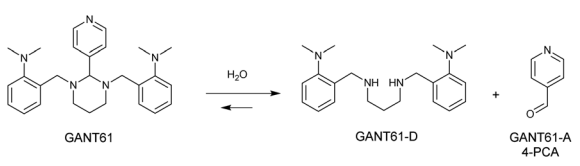

Scheme 1 Hydrolysis of GANT61 to release GANT61-D and 4-PCA.

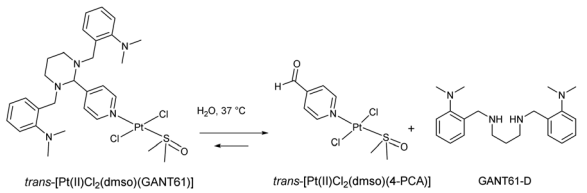

Scheme 2 The proposed hydrolysis of the GANT61 ligand in *trans*-[Pt(II)Cl_2(dmso)(GANT61)] to release hydrolysis products GANT61-D.

Given GANT61 would likely behave as an effective N-donor ligand *via* the pyridyl nitrogen, a *trans* Pt(II) dichlorido, dimethylsulfoxido complex of the Hh pathway inhibitor GANT61, *trans*-[Pt(II)Cl_2(dmso)(GANT61)], was developed. It is expected that the *trans*-Pt(II) GANT61 complex will release the bioactive Hh pathway inhibitor GANT61-D, in a similar manner to GANT61, whilst 4-PCA would remain bound to the Pt(II) centre as the stable amine carrier ligand (Scheme 2).

Herein we report the *in vitro* anti-CSC properties including against CSC-enriched mammospheres and cytotoxicity of the *trans*-Pt GANT61 complex against triple negative breast cancer (TNBC) cells. Furthermore we investigated the potential of this complex to cause DNA damage and inhibit the Hh pathway at the level of GLI.

Results and discussion

Synthesis of *trans*-[Pt(II)Cl_2(dmso)L] type complexes

It is well established that the reaction of one equivalent of an amine N-donor ligand with *cis*-[Pt(II)Cl_2(dmso)$_2$], initially affords the *trans*-isomer of a [Pt(II)Cl_2(dmso)L] type complex, which can be isolated and characterised in full.[22,25,26] Reaction of *cis*-[Pt(II)Cl_2(dmso)$_2$] with either one equivalent of 4-PCA or one equivalent of GANT61 in acetone at rt for 30 minutes afforded either *trans*-[Pt(II)Cl_2(dmso)(4-PCA)] (**1**) and *trans*-[Pt(II)Cl_2(dmso)(GANT61)] (**2**) respectively, Scheme 3.

It is noteworthy that (i) reaction of one equivalent of GANT61 with *cis*-[Pt(II)Cl_2(dmso)$_2$] at an extended reaction time and at reflux will result in the synthesis of the *cis*-isomer, *cis*-[Pt(II)Cl_2(dmso)(GANT61)] and (ii) subsequent reaction of *cis*-[Pt(II)Cl_2(dmso)(GANT61)] with two equivalents of GANT61 affords *cis*-[Pt(II)Cl_2(GANT61)$_2$], which is completely insoluble in aqueous mixtures.[27]

Both **1** and **2** were fully characterised by elemental analysis, ^{1}H NMR, ^{13}C NMR and IR spectroscopy and X-ray crystallography (Fig. S1–S6†).

Briefly with regards to the characterisation of the *trans*-Pt(II) GANT61 complex **2** as a representative example, the elemental analysis was fully consistent with two chlorido ligands, one dmso ligand, one dmso solvent of crystallisation and one GANT61 ligand per Pt(II) centre. In the ^{1}H NMR spectrum of **2**

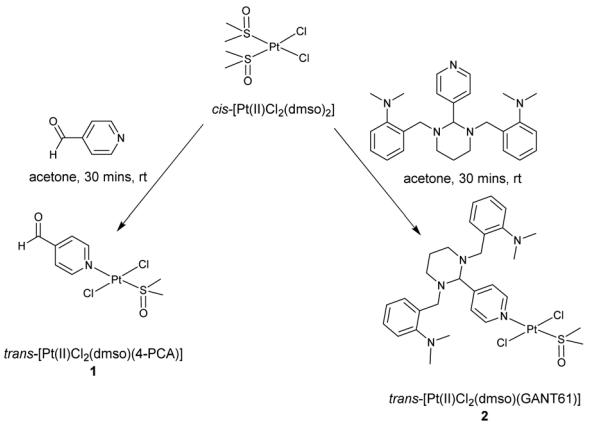

Scheme 3 Synthesis of *trans*-[Pt(II)Cl_2(dmso)L] type complexes **1** and **2** from *cis*-[Pt(II)Cl_2(dmso)$_2$].

($CDCl_3$, Fig. S4†) the twelve aromatic protons associated with the three aromatic rings of GANT61 for example are observed across five signals ranging from 7.01 to 8.63 ppm. Coordination of GANT61 to Pt(II) *via* the pyridyl N-donor atom resulted in a distinctive chemical shift of the two pyridyl aromatic signals from to 7.64 and 8.54 ppm in the free ligand to 7.76 and 8.63 ppm in the complex. The dimethylaniline protons are for instance observed as a singlet at 2.58 ppm and integrate for twelve as expected. The singlet at 3.45 ppm is attributed to the six protons of the coordinated dmso ligand and a second singlet at 2.61 ppm is attributed to the DMSO solvent of crystallisation, which is evidenced in the single X-ray crystal structure. In the ^{13}C NMR spectrum of **2** (Fig. S5†) the aromatic carbons are found between 156 and 119 ppm, the four dimethylaniline (DMA) methyl carbons signal is present at 45 ppm, and the signal for the coordinated dmso methyl carbons at 41 ppm. In the IR spectrum of **2** (Fig. S6†) the distinctive ν(S=O) of the coordinated dmso is observed at 1143 cm^{-1}.

X-ray crystal structures

The X-ray crystal structure of **1** and **2** highlight the *trans* configuration of both Pt complexes, Fig. 2 and 3 with Cl–Pt–Cl

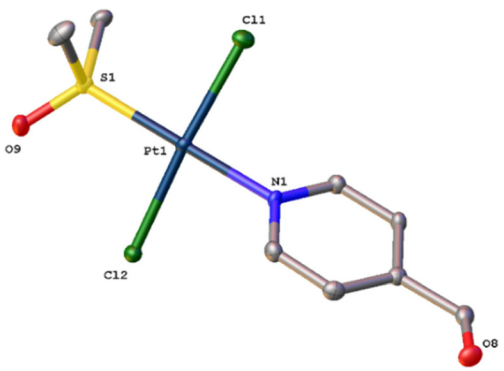

Fig. 2 Molecular structure of **1** with atomic displacement shown at 50% probability. Hydrogen atoms omitted.

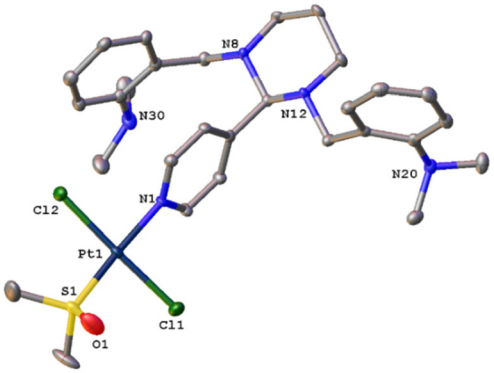

Fig. 3 Molecular structure of **2** with atomic displacement at 50% probability. Hydrogen atoms and mixed partially occupied DMSO/acetone solvent omitted (see ESI† for complete structure).

angles of 175.18(3) Å and 177.37(3) Å respectively. Metal bond lengths are as expected with *trans* substitution. The angle between the pyridine ring plane and the Pt–Cl–S plane is 55.39 (9)° in **1** and 51.85(10)° in **2**. A similar acute angle (*ca.* 59°) is seen in the unsubstituted *trans*-[Pt(II)Cl_2(dmso)(py)] where py is pyridine.[28] In **1**, this twist enables the pyridine ring to form weak hydrogen bonds to the DMSO oxygen. The steric bulk of the GANT61 ligand in **2** forces a more crowded environment, with one dimethylaniline group turned upwards, the other downwards towards the pyridine ring with enough space in the lattice to co-crystallize solvent.

Isomerisation of 1 and 2

Both **1** and **2** were observed to isomerise from the *trans* isomers to the corresponding *cis*-isomers on redissolving the complexes in $CDCl_3$ with stirring at rt. Farrell and coworkers had previously demonstrated the isomerisation in DMSO of *trans*-[Pt(II)Cl_2(dmso)(quinoline)] to *cis*-[Pt(II)Cl_2(dmso)(quinoline)].[22]

The isomerisation can be monitored by ^1H NMR. A downfield shift for example in key aliphatic signals are observed in the ^1H NMR spectra ($CDCl_3$) on the isomerisation of *trans*-[Pt(II)Cl_2(dmso)(GANT61)] to *cis*-[Pt(II)Cl_2(dmso)(GANT61)]. For instance the two sets of CH_2 protons adjacent to the aniline groups shift from 3.68 to 3.83 ppm and the methine proton signal from 4.18 to 4.28 ppm (Fig. S9†).

2 was also observed to isomerise in D_6-DMSO : D_2O (90 : 10) at RT with the same shift in the CH_2 protons adjacent to the aniline groups shift from 3.74 to 4.04 ppm and the methine proton from 4.53 to 4.57 ppm (Fig. S10†).

Hydrolysis of 2 to release GANT61-D

A UV-Vis, HR MS and ^1H NMR study was undertaken to gain an insight into the behaviour of complex **2** in solution (Fig. S10–S12†). With regards to the UV study, **2** is stable in pure DMSO, over a 24 h period. In PBS : DMSO (200 : 1) (Fig. S11†) and DMEM : DMSO (200 : 1) (Fig. S12†) mixtures, **2** is less stable with a decrease in absorption observed, starting after 1 hour and particularly after 8 hours.

After 72 h incubation of **2** in H_2O : DMSO (10 : 1) at 37 °C, ion signals at 534.2197, 612.2338 and 695.2444 amu associated with $[Pt(GANT61–C_6H_5–N(CH_3)_2)(OCH_3)]^+$ ($C_{21}H_{29}N_3OPt$), $[Pt(GANT61–N(CH_3)_2)(OCH_3)]^+$ ($C_{26}H_{33}N_4OPt$) and $[Pt(GANT61)(OCH_3)]^+ + K + H$ ($C_{28}H_{39}N_5OKPt$) were observed in the positive mode of the high resolution mass spectrum (Fig. S13†). In each case, the molecular ions match the expected isotopic pattern and the elemental composition analysis. Furthermore, the peaks match within 10 ppm resolution of the expected values. This shows that some GANT61 remains bound to the Pt(II) centre in aqueous solution. Significantly an ion signal associated with GANT61 + H^+ is clearly observed as the major signal at 341.2703 amu (Fig. S13†) indicating the presence of free bioactive molecule GANT61-D.

An ^{1}H NMR study was undertaken at 37 °C in D_6-DMSO : D_2O (90 : 10) over a 72 hours period. This ^{1}H NMR study is complex and multiple processes are at play over the 72 hours. At time 0 minor additional signals are observed which are not associated with the signals of the parent Pt complex **2** (Fig. S14†). From 1 hour the signals associated with the GANT61 ligand bound to Pt(II), for example the 5 aromatic signals are primarily gone. From 1 hour the evolution of signals associated with a 4-PCA system, *i.e.* two aromatic doublets at 8.22 and 9.22 ppm and an aldehydic proton at 10.44 ppm, with the correct integration are observed. These signals increase up to 72 hours and support the release of GANT61-D, where the 4-PCA is still bound to Pt(II). Signals associated with GANT61-D are also present. For example the aromatic signals for GANT61-D are found from *ca.* 7.46–8.02 ppm though they are poorly resolved.

Collectively, the UV-Vis, HR mass spectrometry and ^{1}H NMR study supports the isomerisation of **2** from *trans* to *cis* and hydrolysis of the GANT61 ligand to release GANT61-D over the 72 experimental time point.

In vitro cytotoxicity

To determine the bulk breast cancer cell and breast CSC potency and investigate potential specificity of the *trans*-Pt(II) GANT61 complex **2**, two human mammary epithelial cell lines were initially used; HMLER and HMLER-shEcad cells. HMLER cells exhibit a stable CSC-like population of 5–8%, whereas HMLER-shEcad cells display a significantly larger CSC-like population (*ca.* 90%).[29]

The *in vitro* cytotoxic properties of Hh pathway inhibitors (GANT61, GANT61-D), 4-PCA, Pt complexes (*trans*-[Pt(II)Cl_2(dmso)(4-PCA)] **1**, *trans*-[Pt(II)Cl_2(dmso)(GANT61)] **2**, cisplatin and carboplatin), and salinomycin against HMLER cells and HMLER-shEcad cells were assessed using the MTT assay. Salinomycin, a breast CSC-specific compound was used as a positive control.[29] Cisplatin and carboplatin were control Pt compounds and 4-PCA a control for the N-donor ligands. The IC_{50} values, the concentration required to reduce viability by 50%, were determined from dose–response curves (Fig. S15–S20†) and are summarized in Table 1.

Both the Hh pathway inhibitor GANT61 and its bioactive hydrolysis product GANT61-D exhibited similar activity against both HMLER and HMLER-shEcad cells with IC_{50} values ranging from 15 to 26 μM. No selectivity for the CSC-enriched HMLER-shEcad cell line over the HMLER cell line was observed for either. 4-PCA was observed to be non-toxic within the concentration range tested (IC_{50} value > 100 μM).

Table 1 IC_{50} values of hedgehog pathway inhibitors (GANT61, GANT61-D), Pt complexes (*trans*-[Pt(II)Cl_2(dmso)(4-PCA)] **1**, *trans*-[Pt(II)Cl_2(dmso)(GANT61)] **2**, cisplatin and carboplatin), 4-PCA and salinomycin against HMLER cells, HMLER-shEcad cells and HMLER-shEcad mammospheres

Compound	HMLER IC_{50} (μM)	HMLER-shEcad IC_{50} (μM)	Mammosphere IC_{50} (μM)
GANT61	16.0 ± 0.6	14.9 ± 0.1	16.0 ± 0.4
GANT61-D	25.8 ± 1.8	23.3 ± 1.2	16.4 ± 1.0
4-PCA	>100	>100	>133
1	36.3 ± 1.9	36.9 ± 0.1	>133
2	1.0 ± 0.02	2.6 ± 0.2	4.4 ± 0.01
Cisplatin[29,30]	2.6 ± 0.02	5.7 ± 0.3	13.5 ± 2.3
Carboplatin[29,30]	67.3 ± 2.8	72.4 ± 8.0	18.1 ± 0.4
Salinomycin[29,30]	11.4 ± 0.4	4.2 ± 0.4	18.5 ± 1.5

It is notable that the *trans*-Pt(II) GANT61 complex **2**, which possesses GANT61, is the most potent of all the test compounds with IC_{50} values of 1.0 and 2.6 μM against HMLER and HMLER-shEcad cells, respectively. No selectivity for the CSC-enriched cells was observed, which is in line with the observation for the Hh pathway inhibitors GANT61 and GANT61-D.

Significantly though *trans*-Pt GANT61 complex **2**, is *ca.* thirty six times more cytotoxic against HMLER and *ca.* fourteen times more cytotoxic against HMLER-shEcad cells as compared to the *trans*-Pt(II) 4-PCA analogue and control compound **1**.

Furthermore **2** has slightly lower IC_{50} values as compared to cisplatin (2.6 & 5.7 μM) and salinomycin (11.4 & 4.2 μM) and considerably lower IC_{50} values as compared to carboplatin (67.3 & 72.4 μM) against HMLER and HMLER-shEcad cells.

Overall, the *in vitro* cytotoxicity data shows that **2** is a potent inhibitor of the growth of breast CSC-depleted HMLER and breast CSC-enriched HMLER-shEcad cells.

Complex **2** did not exhibit notable selectivity for the cancer cells investigated (IC_{50}'s = 1.0 & 2.6 μM) over normal cells, given an IC_{50} of 2.3 ± 0.1 μM (Fig. S11†) was determined against the MCF10A cell line, a human mammary epithelial cell line.

Breast CSCs, due to their stem cell-like character, have the ability to form multicellular three-dimensional structures called mammospheres. The ability of test compounds to reduce CSC-enriched HMLER-shEcad mammosphere formation and viability was assessed using an inverted microscope and the colorimetric resazurin-based reagent TOX8, respectively (Fig. 4 and Table 1).

The addition of GANT61, GANT61-D, 4-PCA, **1**, or **2** (at their IC_{20} values) to single cell suspensions of HMLER-shEcad cells markedly reduced the size of mammospheres formed after 5 days incubation (Fig. 4A). Only the *trans*-Pt(II) GANT61

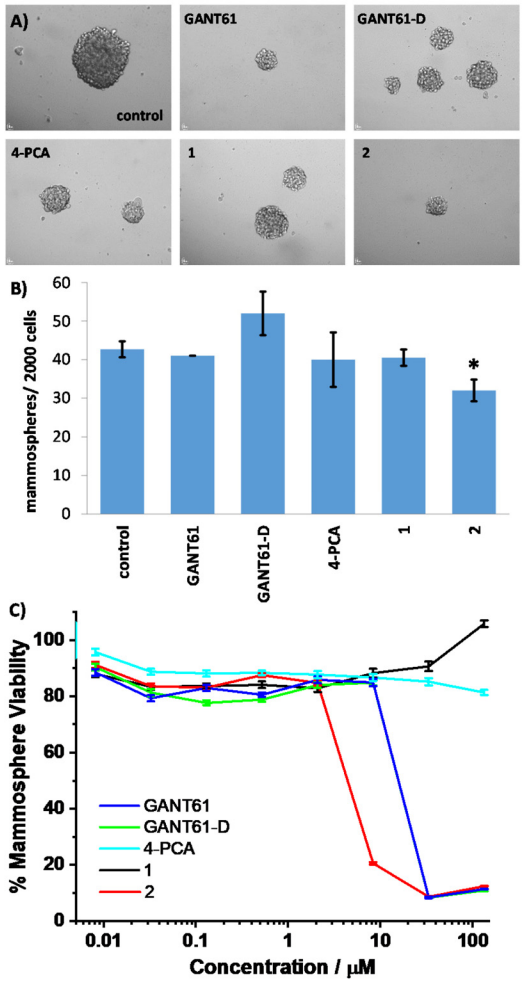

Fig. 4 (A) Representative bright field images (10×) of the mammospheres in the absence and presence of GANT61, GANT61-D, 4-PCA, **1**, or **2** at their respective IC_{20} values, after 5 days incubation. (B) Quantification of mammosphere formation with HMLER-shEcad cells untreated and treated with GANT61, GANT61-D, 4-PCA, **1**, or **2** at their respective IC_{20} values for 5 days. Error bars = SD and Student's *t*-test, * = $p < 0.05$. (C) Representative dose–response curves for the treatment of HMLER-shEcad mammospheres with GANT61, GANT61-D, 4-PCA, **1**, or **2** after 5 days incubation. Error bars = SD.

complex **2** significantly reduced ($p < 0.05$) the number of mammospheres formed (Fig. 4B).

In terms of mammosphere viability, the *trans*-Pt(II) GANT61 complex **2** was the most potent of all the test compounds with an IC_{50} (concentration required to reduce mammosphere viability by 50%) value of 4.4 ± 0.01 μM and was three times more potent than cisplatin (Fig. 4C). The *trans*-Pt(II) GANT61 complex **2** was *ca.* four times more potent towards mammospheres than hedgehog pathway inhibitors GANT61 and GANT61-D (Fig. 4C). Significantly the *trans*-Pt(II) 4-PCA analogue and control compound **1** was not active at the highest concentration investigated, 133 μM (Fig. 4C). Collectively, the mammosphere studies show that **2** is able to markedly reduce breast CSC mammosphere formation, size, and viability.

Cell death analysis

Apoptosis was assessed by flow cytometry using annexin V/PI staining in two TNBC cell lines, MDA-MB-231 (MDA231) and BT549, following treatment with test compounds. TNBC is a highly aggressive subtype of breast cancer that lacks expression of progesterone receptor (PR), estrogen receptor (ER) and human epidermal growth factor 2 (HER2).[31]

The IC_{50} values, the concentration required to induce apoptosis in 50% of cell population, were determined from dose–response curves (Fig. S21†) and are summarized in Table 2.

The BT549 cell line was significantly more sensitive to treatment with all test compounds as compared to the MDA231 cells. Cisplatin was found to be the most potent of the test compounds with IC_{50} values of 2.97 and 0.41 μM against MDA23 and BT549 TNBC cells respectively. Hh pathway inhibitors GANT61 and GANT61-D were relatively non-toxic towards the MDA231 cells in contrast to the cytotoxicity they exhibited against the BT59 cell line with IC_{50}'s of 15.6 and 14.3 μM respectively.

Significantly the *trans*-Pt(II) GANT61 complex **2** exhibited good activity against both cell lines with IC_{50} values of 3.6 and 4.0 μM against MDA231 cells and BT549 cells respectively and was more than 30 times more active than the *trans*-Pt(II) 4-PCA complex **1** against the MDA231 cells and 3 times more active against the BT549 cells.

We hypothesised that a Pt(II) complex possessing GANT61 as an N-donor ligand would release the bioactive Hh pathway inhibitor GANT61-D, in a similar manner to GANT61, whilst 4-PCA would remain bound to the Pt(II) centre as the stable amine carrier ligand. In summary the *trans*-Pt(II) complex **2**, which possesses the Hh pathway inhibitor GANT61 as an N donor ligand exhibits far superior anti-CSC activity including in a CSC-enriched mammosphere model and activity against TNBC cells as compared to its control analogue, the *trans*-Pt(II) 4-PCA complex **1**.

DNA damage and hedgehog pathway inhibition at the level of GLI

We hypothesised that a Pt(II) complex possessing GANT61 as an N-donor ligand should possess DNA binding ability and Hh inhibitory activity. The potential of **2** to damage genomic DNA was probed by monitoring the expression of a biomarker related to the DNA damage pathway using immunoblotting

Table 2 IC_{50} values of hedgehog pathway inhibitors (GANT61, GANT61-D) and Pt complexes (*trans*-[Pt(II)Cl_2(dmso)(4-PCA)] **1**, *trans*-[Pt(II)Cl_2(dmso)(GANT61)] **2** and cisplatin) against MDA231 and BT549 triple negative breast cancer (TNBC) cell lines determined using annexin V-FITC/PI staining and flow cytometry

Compound	MDA231 IC_{50} (μM)	BT549 IC_{50} (μM)
GANT61	>100	15.62
GANT61-D	89.96	14.28
1	>100	12.78
2	3.60	4.00
Cisplatin	2.97	0.41

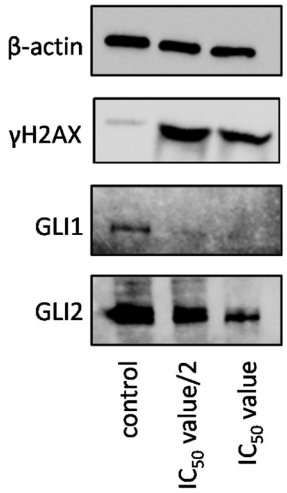

Fig. 5 Immunoblotting analysis of proteins related to the DNA damage and GLI pathways. Protein expression in HMLER-shEcad cells following treatment with **2** (IC_{50}/2 value and IC_{50} value for 72 h).

methods. HMLER-shEcad cells incubated with **2** (IC_{50}/2 & IC_{50} for 72 h) displayed a marked increase in the expression of the phosphorylated form of H2AX (γH2AX), indicative of DNA damage (Fig. 5).

HMLER-shEcad cells treated with **2** (IC_{50}/2 & IC_{50} for 72 h) also exhibited decreased expression of GLI-1 and GLI-2 (Fig. 5). As previously highlighted, GANT61 inhibits the Hh pathway downstream at the level of GLI. It has been shown to block GLI function in the nucleus, suppress both GLI1- and GLI2-mediated transcription, and inhibit the binding of GLI1 with DNA.[13,14]

In summary the *trans*-Pt GANT61 complex **2** has been shown to cause DNA damage and inhibit the Hh pathway at the level of GLI.

Experimental

Materials and instrumentation

Potassium tetrachloroplatinate(II) was purchased from Alfa Aesar (Heysham LA3 2XY, United Kingdom) and used without further purification. All other commercially available reagents and solvents, including deuterated solvents, were purchased from Merck/Sigma-Aldrich (Arklow, Co. Wicklow, Ireland), and used without further purification unless otherwise stated. GANT61,[32] GANT61-D[32] and *cis*-[Pt(II)Cl_2(dmso)$_2$][33] were synthesised as previously reported. ^{1}H NMR and ^{13}C NMR spectra were recorded on a Bruker Avance 400 NMR spectrometer. The spectra were analysed using MestReNova software. The residual undeuterated solvent signals were used as internal references.[34] Elemental analysis (C, H, N and Cl) was performed at the Microanalytical Laboratory, School of Chemistry and Chemical Biology, University College Dublin, Ireland. Fourier Transform Infrared (FT-IR) spectra were recorded in-house using a Nicolet iS10 FT-IR spectrometer with spectra recorded from 4000–400 wavenumbers (cm^{-1}) and analysed using OMNICTM software.

Synthetic procedures

***trans*-[Pt(II)Cl_2(dmso)(4-PCA)] (1).** 4-Pyridinecarboxaldehyde (4-PCA) (111 μL, 1.18 mmol) was added to a suspension of *cis*-[Pt(II)Cl_2(dmso)$_2$] (500 mg, 1.18 mmol) in acetone (20 mL). Following addition the white, cloudy suspension gradually turned clear and yellow. After 30 min of stirring at rt, the reaction was filtered under gravity, concentrated *in vacuo* to *ca.* 10 mL, and stored at 4 °C for 1.5 h. The resulting precipitate revealed **1** as a crystalline, bright yellow solid (365.8 mg, 69%) which was collected *via* vacuum filtration. A single crystal suitable for X-ray crystallography was collected following recrystallisation in chloroform *via* slow evaporation at rt.

^{1}H NMR (400 MHz, $CDCl_3$) δ 10.14 (s, 1H), 9.07 (d, J = 4.0 Hz, 2H), 7.86 (d, J = 4.0 Hz, 2H), 3.49 (s, 6H). ^{13}C NMR (100 MHz, $CDCl_3$) δ 188.99 (s), 153.80 (s), 142.93 (s), 123.97 (s), 44.34 (s). $C_8H_{11}Cl_2NO_2PtS$ requires C, 21.29; H, 2.46; N, 3.10; Cl, 15.71%, found C, 21.30; H, 2.33; N, 2.86; Cl, 15.74%. FT-IR ν_{max} (cm^{-1}): 3105.1, 1714.4 ν(C═O), 1424.3, 1319.2, 1139.0 ν(S═O), 1026.1, 820.4.

***trans*-[Pt(II)Cl_2(dmso)(GANT61)] (2).** A solution of GANT61 (198.0 mg; 0.47 mmol) in acetone (6 mL) was added dropwise to a suspension of *cis*-[Pt(II)Cl_2(dmso)$_2$] (201.5 mg; 0.47 mmol) in acetone (10 mL). The suspension gradually turned clear and yellow. After 30 min of stirring at rt, the reaction was filtered under gravity and concentrated *in vacuo* to *ca.* 1 mL. The concentrated yellow solution was then scratched and a few drops of ether was added. The solution was left to stand at 4 °C for 5 h to precipitate **2** as bright yellow crystals (274.8 mg; 74%). A single crystal suitable for X-ray crystallography was isolated.

^{1}H NMR (400 MHz, $CDCl_3$) δ 8.63 (d, J = 4.0 Hz, 2H), 7.76 (d, J = 4.0 Hz, 2H), 7.46 (d, J = 8.0 Hz, 2H), 7.20–7.17 (m, 2H), 7.05–7.01 (m, 4H), 4.18 (s, 1H), 3.72 (dd, J = 20 Hz, 12 Hz, 4H), 3.45 (s, 6H), 2.93–2.89 (m, 2H), 2.61 (s, 6H), 2.58 (s, 12H), 2.43–2.38 (m, 2H), 1.83–1.82 (m, 1H), 1.48–1.46 (m, 1H). ^{13}C NMR (100 MHz, $CDCl_3$) δ 156.75, 153.04, 151.30, 133.26, 129.57, 127.66, 126.27, 123.29, 119.21, 83.10, 52.96, 48.97, 45.30, 44.30, 41.14, 20.94. $C_{29}H_{41}Cl_2N_5OPtS{\cdot}SO(CH_3)_2$ requires C, 43.71; H, 5.56; N, 8.22; Cl, 8.32%, found C, 44.16; H, 5.48; N, 8.05; Cl, 8.45%. FT-IR ν_{max} (cm^{-1}): 2942.9, 2792.4, 1491.6, 1301.3, 1142.8 ν(S═O), 1035.1, 936.9.

X-ray crystallography

Data for **1** were collected on a Bruker APEX DUO and for **2** on a Bruker D8 Quest ECO using Mo Kα radiation (λ = 0.71073 Å). Each sample was mounted on a MiTeGen cryoloop and data collected at 100(2) K. Bruker APEX software[35] was used to collect and reduce data. Absorption corrections were applied using SADABS.[36] Structures were solved with the SHELXT structure solution program[37] using Intrinsic Phasing. Data were refined using least squares method on F^2 with SHELXL.[38] All non-hydrogen atoms were refined anisotropically. Hydrogen atoms were assigned to calculated positions using a riding model with appropriately fixed isotropic thermal parameters. Molecular

graphics were generated using OLEX2.[39] Crystal data, details of data collection and refinement are given in Table S1.†

Disordered solvents are present in the void in **2** with DMSO, 60% occupied and acetone, 15% occupied. Both modelled with a rigid model. Displacement constraints (EADP) were used to model the oxygen and carbon atoms. The large residual density is located near the heavy Pt atom in both **1** and **2**, and the intensity (1.2 and 1.64 e $Å^{-3}$, 0.61 Å and 0.93 Å from Pt1 in both **1** and **2**) is smaller than the $0.1 \times Z$ e $Å^{-3}$ (Z = 78 for Pt). This originates from absorption. The deepest hole is −1.43 and −1.15 e $Å^{-3}$, 0.73 Å and 1.13 Å from Pt1 and C19 respectively in **1** and **2**.

Crystallographic data for the structure in this paper have been deposited with the Cambridge Crystallographic Data Centre as supplementary publication no. 2196198 and 2196199.†

Cell lines and cell culture conditions

The human mammary epithelial cell lines, HMLER and HMLER-shEcad were kindly donated by Prof. R. A. Weinberg (Whitehead Institute, MIT). The human epithelial breast MCF710A cell line was acquired from the American Type Culture Collection (ATCC, Manassas, VA, USA). HMLER, HMLER-shEcad, and MCF10A cells were maintained in Mammary Epithelial Cell Growth Medium (MEGM) with supplements and growth factors (BPE, hydrocortisone, hEGF, insulin, and gentamicin/amphotericin-B). The cells were grown at 310 K in a humidified atmosphere containing 5% CO_2.

Cytotoxicity MTT assay

The colorimetric MTT assay was used to determine the toxicity of GANT61, GANT61-D, 4-PCA, **1**, and **2**. HMLER, HMLER-shEcad, and MCF10A cells (5×10^3) were seeded in each well of a 96-well plate. After incubating the cells overnight, various concentrations of the compounds (0.0004–100 μM), were added and incubated for 72 h (total volume 200 μL). Stock solutions of the compounds were prepared as 10 mM solutions in DMSO and diluted using media. The final concentration of DMSO in each well was 0.5% and this amount was present in the untreated control as well. After 72 h, 20 μL of a 4 mg mL^{-1} solution of MTT in PBS was added to each well, and the plate was incubated for an additional 4 h. The MEGM/MTT mixture was aspirated and 200 μL of DMSO was added to dissolve the resulting purple formazan crystals. The absorbance of the solutions in each well was read at 550 nm. Absorbance values were normalised to (DMSO-containing) control wells and plotted as concentration of test compound *versus* % cell viability. IC_{50} values were interpolated from the resulting dose dependent curves. The reported IC_{50} values are the average of three independent experiments (n = 18).

Tumorsphere formation and viability assay

HMLER-shEcad cells (5×10^3) were plated in ultralow-attachment 96-well plates (Corning) and incubated in MEGM supplemented with B27 (Invitrogen), 20 ng mL^{-1} EGF, and 4 μg mL^{-1} heparin (Sigma) for 5 days. Studies were also conducted in the presence of GANT61, GANT61-D, 4-PCA, **1**, and **2** (0–133 μM). Mammospheres treated with GANT61, GANT61-D, 4-PCA, **1**, and **2** (at their respective IC_{20} values, 5 days) were counted and imaged using an inverted microscope. The viability of the mammospheres was determined by addition of a resazurin-based reagent, TOX8 (Sigma). After incubation for 16 h, the fluorescence of the solutions was read at 590 nm (λ_{ex} = 560 nm). Fluorescence values were normalised to DMSO-containing controls and plotted as concentration of test compound *versus* % mammospheres viability. IC_{50} values were interpolated from the resulting dose dependent curves. The reported IC_{50} values are the average of two independent experiments, each consisting of two replicates per concentration level (overall n = 4). The microscope used for this study is a Nikon TE300 semi-automatic microscope with automated shutters and filter wheels and manual XY control. The imaging part of the system is automated and controlled by Improvision's Openlab software, running on a Mac (OS X).

Annexin V-FITC/PI cell viability assay

MDA231 and BT549 cells were seeded at 4.5×10^4 cells in a 24 well plate for 24 h prior to treating with cisplatin, GANT61, GANT61-D, **1** and **2** at stated doses for 48 h. Apoptosis was assessed by annexin V-FITC/propidium iodide staining. The cells were collected, washed with PBS and resuspended in annexin V binding buffer (10 mM Hepes pH 7.4, 140 mM NaCl and 2.5 mM $CaCl_2$) and annexin V-FITX (0.25 mg ml^{-1} BioLegend, 640906, Sigma-Aldrich P4170) and PI (1 mg ml^{-1}) was added to each sample. Cell viability was determined by flow cytometry on the Biosciences LSR II flow cytometer. Viability is shown normalised to DMSO control. Dose–response curves and IC_{50}'s were fitted using nonlinear regression in GraphPad Prism 9.

Immunoblotting analysis

HMLER-shEcad cells (5×10^3 cells) were incubated with **2** ($IC_{50}/2$ & IC_{50} for 72 h) at 37 °C. Cells were washed with PBS, scraped into SDS-PAGE loading buffer (64 mM Tris–HCl (pH 6.8)/9.6% glycerol/2% SDS/5% β-mercaptoethanol/0.01% bromophenol blue), and incubated at 95 °C for 10 min. Whole cell lysates were resolved by 4–20% sodium dodecylsulphate polyacylamide gel electrophoresis (SDS-PAGE; 200 V for 25 min) followed by electro transfer to polyvinylidene difluoride membrane, PVDF (350 mA for 1 h). Membranes were blocked in 5% (w/v) non-fat milk in PBST (PBS/0.1% Tween 20) and incubated with the appropriate primary antibodies (Cell Signalling Technology). After incubation with horseradish peroxidase-conjugated secondary antibodies (Cell Signalling Technology), immune complexes were detected with the ECL detection reagent (BioRad) and analysed using a chemiluminescence imager (Bio-Rad ChemiDoc Imaging System).

Conclusions

In summary, we present a novel *trans*-Pt(II) complex of the Hh pathway inhibitor GANT61, *trans*-[Pt(II)Cl_2(dmso)(GANT61)] **2**.

This complex does undergo isomerisation from *trans*- to *cis*-in solution and therefore the biological activity of **2** is also associated with the *cis*-configuration. This complex is a potent inhibitor of the growth of breast CSC-depleted HMLER and breast CSC-enriched HMLER-shEcad cells. Furthermore **2** markedly reduced the size and viability and significantly reduced the number of CSC-enriched HMLER-shEcad mammospheres formed. **2** also induced apoptosis with low micromolar IC_{50} values against two TNBC cell lines, MDA-MB-231 (MDA231) and BT549 **2**, which possesses the Hh pathway inhibitor GANT61 as an N donor ligand exhibits far superior anti-CSC activity including in the CSC-enriched mammosphere model and activity against TNBC cells as compared to its control analogue, the *trans*-Pt(II) 4-PCA complex **1**.

We hypothesised that the *trans*-Pt(II) GANT61 complex would release the bioactive Hh pathway inhibitor GANT61-D, in a similar manner to GANT61, whilst 4-PCA would remain bound to the Pt(II) centre as the stable amine carrier ligand. The *trans*-Pt(II) complex **2**, was shown to release GANT61 over a 72 hours timepoint in solution and to cause DNA damage and inhibit the Hh pathway at the level of GLI in HMLER-shEcad cells.

The Hh pathway inhibitor GANT61 enhances the cytotoxicity of the *trans*-[Pt(II)Cl_2(dmso)L] class of Pt complex towards breast cancer stem cells and triple negative breast cancer cells. Ultimately hedgehog pathway inhibition may ameliorate the anticancer activity of the many different classes of Pt(II) complexes.

Author contributions

Aisling L. Ryan: conceptualisation, methodology, investigation, writing – original draft preparation, funding acquisition. Joshua Northcote-Smith: methodology, investigation. Aoife McKeon: conceptualisation, methodology, investigation. Andrew Roe: methodology, investigation, writing – review and editing. Paul O'Dowd: methodology, investigation. Brendan Twamley: methodology, resources, writing – original draft preparation. Triona Ní Chonghaile: methodology, resources, writing – review and editing. Kogularamanan Suntharalingam: conceptualisation, resources, methodology, writing – original draft preparation. Darren M. Griffith: conceptualisation, resources, methodology, writing – original draft preparation, supervision, project administration, funding acquisition.

Conflicts of interest

There are no conflicts to declare.

Acknowledgements

ALR sincerely thanks the Irish Research Council (GOIPG/2017/1384) for financial support. DMG and POD gratefully acknowledges funding received from the Synthesis and Solid State Pharmaceutical Centre (SSPC), financed by a research grant from Science Foundation Ireland (SFI) and co-funded under the European Regional Development Fund under Grant Number 12/RC/2275_P2. AM and DG are also funded by a research grant from SFI under Grant Number 12/IP/1305. KS and JNS thank EPSRC (EP/S005544/1) and the University of Leicester for funding. TNC and AR are funded by SFI under grant number 19/FFP/6461.

References

1 S. Rottenberg, C. Disler and P. Perego, *Nat. Rev. Cancer*, 2021, **21**, 37–50.
2 S. Alassadi, M. J. Pisani and N. J. Wheate, *Dalton Trans.*, 2022, **51**, 10835–10846.
3 R. Oun, Y. E. Moussa and N. J. Wheate, *Dalton Trans.*, 2018, **47**, 6645–6653.
4 J. Zhou, Y. Kang, L. Chen, H. Wang, J. Liu, S. Zeng and L. Yu, *Front. Pharmacol.*, 2020, **11**, 343.
5 L. Yang, H.-J. Xie, Y.-Y. Li, X. Wang, X.-X. Liu and J. Mai, *Oncol. Rep.*, 2022, **47**, 82.
6 C. Correia, T. M. Weiskittel, C. Y. Ung, J. C. Villasboas Bisneto, D. D. Billadeau, S. H. Kaufmann and H. Li, *Front. Cell Dev. Biol.*, 2022, **10**, 752326.
7 F. Tomao, A. Papa, L. Rossi, M. Strudel, P. Vici, G. Lo Russo and S. Tomao, *J. Exp. Clin. Cancer Res.*, 2013, **32**, 48.
8 S. Muñoz-Galván and A. Carnero, *Cells*, 2020, **9**(6), 1402.
9 N. M. Nguyen and J. Cho, *Int. J. Mol. Sci.*, 2022, **23**, 1733.
10 B. Aramini, V. Masciale, G. Grisendi, F. Bertolini, M. Maur, G. Guaitoli, I. Chrystel, U. Morandi, F. Stella, M. Dominici and K. H. Haider, *Cancers*, 2022, **14**(4), 976.
11 K. Song and M. Farzaneh, *Stem Cell Res. Ther.*, 2021, **12**, 245.
12 T. Zhang, H. Zhou, K. Wang, X. Wang, M. Wang, W. Zhao, X. Xi, Y. Li, M. Cai, W. Zhao, Y. Xu and R. Shao, *Biomed. Pharmacother.*, 2022, **147**, 112616.
13 M. Lauth, Å. Bergström, T. Shimokawa and R. Toftgård, *Proc. Natl. Acad. Sci. U. S. A.*, 2007, **104**, 8455–8460.
14 A. Agyeman, B. K. Jha, T. Mazumdar and J. A. Houghton, *Oncotarget*, 2014, **5**, 4492.
15 T. Mazumdar, J. DeVecchio, A. Agyeman, T. Shi and J. A. Houghton, *Cancer Res.*, 2011, **71**, 5904–5914.
16 T. Mazumdar, J. DeVecchio, T. Shi, J. Jones, A. Agyeman and J. A. Houghton, *Cancer Res.*, 2011, **71**, 1092–1102.
17 P. Bhateja, M. Cherian, S. Majumder and B. Ramaswamy, *Cancers*, 2019, **11**, 1126.
18 M. Lauth, V. Rohnalter, A. Bergstrom, M. Kooshesh, P. Svenningsson and R. Toftgard, *Mol. Pharmacol.*, 2010, **78**(3), 486–496.
19 A. Calcaterra, V. Iovine, B. Botta, D. Quaglio, I. D'Acquarica, A. Ciogli, A. Iazzetti, R. Alfonsi, L. Lospinoso Severini and P. Infante, *J. Enzyme Inhib. Med. Chem.*, 2018, **33**, 349–358.
20 A. L. Ryan, M.-C. Fitzgerald, A. Ozsváth, B. Twamley, P. Buglyó, B. M. Murphy and D. M. Griffith, *Inorg. Chem.*, 2019, **58**, 16075–16086.

21 J. J. Wilson and S. J. Lippard, *Chem. Rev.*, 2014, **114**, 4470–4495.
22 M. Van Beusichem and N. Farrell, *Inorg. Chem.*, 1992, **31**, 634–639.
23 G. Giannikopoulos, C.-L. Teo, M. D. Hall, R. R. Fenton and T. W. Hambley, *Aust. J. Chem.*, 2003, **56**, 685–689.
24 N. Farrell, L. R. Kelland, J. D. Roberts and M. Van Beusichem, *Cancer Res.*, 1992, **52**, 5065–5072.
25 P.-C. Kong, D. Iyamuremye and F. D. Rochon, *Bioinorg. Chem.*, 1976, **6**, 83–89.
26 L. G. Marzilli, Y. Hayden and M. D. Reily, *Inorg. Chem.*, 1986, **25**, 974–978.
27 A. McKeon, *PhD thesis*, Royal College of Surgeons in Irelands, 2017.
28 F. Caruso, R. Spagna and L. Zambonelli, *Acta Crystallogr., Sect. B: Struct. Crystallogr. Cryst. Chem.*, 1980, **36**, 713–715.
29 P. B. Gupta, T. T. Onder, G. Jiang, K. Tao, C. Kuperwasser, R. A. Weinberg and E. S. Lander, *Cell*, 2009, **138**, 645–659.
30 A. Eskandari, A. Kundu, S. Ghosh and K. Suntharalingam, *Angew. Chem., Int. Ed.*, 2019, **58**, 12059–12064.
31 C. M. Perou, T. Sørlie, M. B. Eisen, M. van de Rijn, S. S. Jeffrey, C. A. Rees, J. R. Pollack, D. T. Ross, H. Johnsen, L. A. Akslen, Ø. Fluge, A. Pergamenschikov, C. Williams, S. X. Zhu, P. E. Lønning, A.-L. Børresen-Dale, P. O. Brown and D. Botstein, *Nature*, 2000, **406**, 747–752.
32 V. Chenna, C. Hu and S. R. Khan, *J. Environ. Sci. Health, Part A: Toxic/Hazard. Subst. Environ. Eng.*, 2014, **49**, 641–647.
33 V. Y. Kukushkin, A. J. L. Pombeiro, C. M. P. Ferreira and L. I. Elding, *Inorg. Synth.*, 2002, **33**, 189–196.
34 G. R. Fulmer, A. J. M. Miller, N. H. Sherden, H. E. Gottlieb, A. Nudelman, B. M. Stoltz, J. E. Bercaw and K. I. Goldberg, *Organometallics*, 2010, **29**, 2176–2179.
35 Bruker, *APEX3 v2017.3-0*, Bruker AXS Inc., Madison, WI, USA, 2017.
36 L. Krause, R. Herbst-Irmer, G. M. Sheldrick and D. Stalke, *J. Appl. Crystallogr.*, 2015, **48**, 3–10.
37 G. Sheldrick, *Acta Crystallogr., Sect. A: Found. Adv.*, 2015, **71**, 3–8.
38 G. Sheldrick, *Acta Crystallogr., Sect. C: Struct. Chem.*, 2015, **71**, 3–8.
39 O. V. Dolomanov, L. J. Bourhis, R. J. Gildea, J. A. K. Howard and H. Puschmann, *J. Appl. Crystallogr.*, 2009, **42**, 339–341.